IOPscience iopscience.iop.org

Home Search Collections Journals About Contact us My IOPscience

Electronic structures of point defects in III-V compound semiconductors

This article has been downloaded from IOPscience. Please scroll down to see the full text article.

1989 J. Phys.: Condens. Matter 1 7347

(http://iopscience.iop.org/0953-8984/1/40/010)

View the table of contents for this issue, or go to the journal homepage for more

Download details:
IP Address: 171.66.16.96
The article was downloaded on 10/05/2010 at 20:23

Please note that terms and conditions apply.

J. Phys.: Condens. Matter 1 (1989) 7347–7366. Printed in the UK

Electronic structures of point defects in III–V compound semiconductors

M J Puska
Laboratory of Physics, Helsinki University of Technology, 02150 Espoo, Finland

Received 23 February 1989

Abstract. The self-consistent electronic structures of ideal vacancies in nine III–V compound semiconductors and in Si and Ge have been calculated using the spin-unrestricted density-functional theory and the linear muffin-tin-orbital Green function method. Moreover, anti-site defects in these compound semiconductors have been investigated. The ionisation levels in the band gap have been determined from the total energies for all types of vacancies in different charge states. The trends in the ionisation level positions are studied when the width of the band gap and the 'size' of the vacancy are varying from one host to another. The results are compared with previous calculations and experiments, and the effects due to lattice relaxation are discussed.

1. Introduction

Point defects have a crucial role in determining the optical and electrical properties of semiconductors, and therefore the understanding of their electronic structures, their behaviour under different conditions, and especially their microscopic identification are of great importance for pure and applied semiconductor physics [1, 2]. One of the important issues is the deep levels in the band gap, induced by defects [3, 4]. They are localised electron states, which may trap charge carriers. Their energetics are characterised by ionisation levels, i.e. those positions of the equilibrium Fermi level at which the occupation of the deep level, and thus also the charge of the defect, change. Many experimental techniques, e.g. deep-level-transient spectroscopy, optical methods and electron spin resonance techniques, can measure the positions of the ionisation levels, and can thereby provide information for the identification of the corresponding defect [3]. Theoretical calculations which can predict the deep-level energetics and symmetry properties are essential for achieving this goal.

Vacancies and anti-sites are among the most important native defects in semiconductors. In this paper we present theoretical results for ideal (non-relaxed) vacancies and anti-sites in nine different compound semiconductors. Vacancies in Si and Ge are also calculated. The purpose is to provide a consistent data basis for the ionisation levels and thereby enable comparisons and studies of trends between different hosts. The calculations without lattice relaxation are valuable, because the unambiguous determination of the relaxation by total energy methods is still a difficult task [5] and not amenable to systematic trend studies. Moreover, due to previous controversial theoretical results for some important unrelaxed defects a recalculation by a new type of method is called for. The knowledge of the ionisation levels for vacancies is especially

0953-8984/89/407347+20$02.50 © 1989 IOP Publishing Ltd

important for the defect studies by positron lifetime spectroscopy [6, 7]. This is because the method is sensitive only to vacancies which are negative or neutral; positively charged vacancies are excluded due to the strong Coulomb repulsion.

In this work we use the linear muffin-tin-orbital method (LMTO) [8, 9] to calculate the self-consistent electronic structures for bulk semiconductors, and the corresponding Green function scheme [10] is employed in the case of vacancies. The atomic-sphere approximation (ASA) is used throughout. Previously the deep levels have been predicted within the density fuctional approach by using the pseudopotential or cluster approaches. An LMTO ASA scheme has been applied before in the case of point defects in semiconductors to calculate the properties of chalcogen [11] and transition-metal [12] impurities in Si. The method has previously been used for vacancies in Si and GaAs, but the ionisation levels were not determined at that time [13]. One of the benefits of the LMTO method (cf the pseudopotential methods) is that it provides a unified basis for calculating the electronic properties of materials consisting from different elements, and thereby the LMTO method enables comparisons between different semiconductors.

In §2 we shall briefly describe the most important points of our Green function approach. The technical aspects have already been published elsewhere [10, 13]. The results are presented in §3, where they are also discussed and compared with experiments and previous theoretical works. Section 4 contains the conclusions.

2. Calculation scheme

The calculations are based on the density-functional approach, and involve two kinds of approximations. The first deal with electronic exchange and correlation, while the second are related to the solution of the one-particle Kohn–Sham equations in the relevant geometry. In this work we have made the following approximations: (i) the local-density approximation (LDA) for the electron exchange and correlation and (ii) the frozen-core approximation are the fundamental ones. The more technical approximations are (iii) the linearisation in LMTO and (iv) the atomic-sphere approximation (ASA). An important related issue is the correction of the energy gap widths by (v) the 'scissors' operator [14]. In this section we first describe these approximations and then give a general outline of the Green function method. A more complete description of the technical details of the present method can be found in [13].

The spin-unrestricted density functional formalism is used for defect calculations which, because of the occupation of the deep levels according to Hund's rules, lead to different spin-up and spin-down densities. The exchange–correlation energy and potential are calculated from an interpolation equation based on Ceperley and Alder's many-body calculations [15]. The valence electron density is calculated self-consistently, but in the frozen-core approximation the atomic orbitals are used for the core electrons in the solid.

The linearisation in LMTO [8, 9] means that the spherical (in our calculations, scalar relativistic) Schrödinger equation inside an atomic sphere (see ASA below) is solved exactly only for one energy $E_{\nu \boldsymbol{R}l}$, which depends on the site $\boldsymbol{R}$ and on the angular momentum quantum number l. In this work the $E_{\nu \boldsymbol{R}l}$ are chosen to coincide with the centre of mass of the $\boldsymbol{R}l$ projection of the valence charge, except for the cases where the d component for the group III atom is shifted to higher energies in order to avoid the so-called 'ghost' bands. The wavefunctions around E_{ν} are calculated

using the first-order Taylor expansion in $(E - E_v)$. Because the variational principle is used in constructing the (Bloch symmetry) wavefunctions in the crystal lattice, the energy eigenvalues (the band structure), and the wavefunctions are in fact correct to second order, $(E - E_v)^2$. The energy eigenvalues can be corrected to third order by a perturbative method but, because for the calculation of the Green function we want the energy eigenvalues and wavefunctions to be consistent, this step is not taken.

The most severe approximation made is the ASA. This approximation means that potentials and charge densities are spherical averages within spheres. The spheres fill the whole crystal space leaving no interstitial space. In this work the systems have a zincblende (or diamond) structure and we use four spheres per unit cell. Two of them are centred at host nuclei and two are at tetrahedral interstitial sites. For simplicity, all spheres have equal radii and in all of them the wavefunctions are described using s, p and d partial waves.

It is well known that the density-functional theory in LDA predicts minimum band gaps which are typically of the order of 50% too small [16]. This is a serious flaw in applications where one is interested in bound states *within* the band gap. To remedy this, we use the simple 'scissors' operator [14], i.e. we shift the conduction bands rigidly to obtain the experimental band gap before calculating the unperturbed Green function. The scissors operator merely shifts the energy zero and thus the wavefunctions used in calculating the Green function are not affected. The validity of the scissors operator requires that the differences between the true quasiparticle energy bands and the density-functional LDA bands do not depend strongly on the $\boldsymbol{k}$-vector and energy. According to a recent calculation [17], this is true within 0.1, 0.2, 0.2 and 0.4 eV for the uppermost valence band and the lowest conduction band in Si, GaAs, AlAs and C, respectively. Thus the situation is quite satisfactory, except perhaps for C which, on the other hand, has a wide band gap of 5.5 eV.

With these approximations we first calculate the self-consistent band structures of the perfect crystal lattices. The imaginary part of the unperturbed Green function G_0 is proportional to the unperturbed projected density of states (DOS) N_0

$$\operatorname{Im} G_0(E) = \pi N_0(E) \tag{1}$$

and the real and imaginary parts of the Green function can be calculated for a general point z in the complex energy plane by the Hilbert transform

$$G_0(z) = \int_{-\infty}^{\infty} \frac{N_0(E')}{z - E'} \, \mathrm{d}E'. \tag{2}$$

A point defect induces a perturbed region in the host. In the case of a vacancy in a zincblende structure a sphere containing the host atom is substituted by an 'empty' sphere. The Green function G for the perturbed system is obtained by solving the Dyson equation

$$(1 + G_0 \Delta V)G = G_0 \tag{3}$$

where ΔV is a defect-induced perturbation in the effective potential. Due to screening the perturbation in the potential is well localised. In practice therefore, we choose the perturbed region to consist only of the central defect sphere, the four empty spheres and four nearest-neighbour atom spheres adjacent to it. The electron density and the defect-induced potential are solved self-consistently in an iteration loop: we start from

a guessed potential and insert that in the Dyson equation, which gives the perturbed Green function. The imaginary part is then used to calculate the perturbed density of states (DOS) and the electron density. The electron density determines the new potential, which is used to start the next iteration. Iterations are continued until self-consistency is achieved in the electron structure.

The benefit of the Green function method is that although the perturbed region is limited, single-particle wavefunctions can extend beyond it. The electrons bound at deep levels in vacancies are localised so that typically in our ASA calculations only about 30% of the electron is in the perturbed region, mainly in the atomic spheres adjacent to the vacancy sphere. (There the charge has a strong p character around the nuclei, and thus this distribution reflects the charge accumulation into the dangling bonds.) This should be contrasted with cluster calculations for point defects, where the confinement of the wavefunctions in the cluster may cause spurious results.

In practical calculations [13] the values of the unperturbed Green function along the integration path on the complex energy plane are calculated from the projected number of states (NOS) (= integrated density of states (DOS)) on the real energy axis using the Hilbert transform. The use of NOS instead of DOS reduces considerably the number of points needed in the Hilbert transform. The use of the complex energy integration path makes possible an accurate calculation of the electron density in perfect and perturbed systems with few energy points. Another commonly used scheme is to calculate the real and imaginary parts of the Green function on the complex plane directly from the unperturbed wavefunctions and band structure, but the use of the Hilbert transform is in our case faster. The electron densities corresponding to both the delocalised states and the bound states are calculated by integrating along the path in the complex energy plane. The energy eigenvalues of the bound states are determined by searching in the band gap for the zeros of the determinant of the matrix multiplying the perturbed Green function in the Dyson equation (3).

In the case of charged defects the long-range Coulomb potential causes additional complications, because in the calculations the changes in the potential are limited in the perturbed region. We have taken the effects due to the Coulomb tail into account by shifting the potential in the perturbed region by the amount of Q/ϵ eV (see [18]). Here Q is the charge of the defect and ϵ the static dielectric constant of the host semiconductor. In the case of Si this shift is about 0.1 eV per unit change in the charge state. The scaling by the dielectric constant gives slight variations between different materials.

The ionisation levels for defects in semiconductors are determined as those positions of the chemical potential (Fermi level), at which the charge of the defect in the stable state changes. The ionisation levels can be calculated from the density-functional total energies of the defect in different charge states [19]. Actually, these energies are the defect-induced changes in total energy of the infinite system. The total energy $\Delta E(N,\mu)$ for the defect with charge Q depends on the position of the chemical potential μ as

$$\Delta E(Q,\mu) = \Delta E(Q,\epsilon_v^*) + Q(\mu - \epsilon_v^*) \tag{4}$$

where $\Delta E(Q,\epsilon_v^*)$ is the total energy given by the Green function method with the chemical potential at ϵ_v^*, which is the end point of the energy integration loop around the valence band. ϵ_v^* is in the band gap just above the top of the valence band. Equation (4) means that there is a reservoir of electrons at the energy μ. In the case of a positive defect ($Q > 0$) we have to raise Q electrons to this reservoir, and therefore for a positive

defect $\Delta E(Q, \mu)$ is a linear function of μ increasing with the slope Q. Similarly, we get a linearly decreasing function for negative defects ($Q < 0$), and a constant for a neutral defect. The ionisation level $(Q + 1, Q)$ is then the solution of

$$\Delta E(Q + 1, \mu) = \Delta E(Q, \mu) \tag{5}$$

with respect to μ. The ionisation levels are obtained as a difference between two total energies. Therefore we expect that errors originating e.g. from ASA should largely cancel.

3. Results and discussion

3.1. *Perfect lattice electron structures*

The relevant experimental data [20], i.e. lattice constants, band gaps and dielectric constants for the investigated semiconductors are collected in table 1.

Table 1. Data for semiconductors used in the calculations [20]. The experimental lattice constants a, experimental band gaps E_g^{exp} and its character, i.e. direct (d) or indirect (i), and the dielectric constants ϵ are given. The theoretical band gaps E_g^{theor} resulting from our second order LMTO ASA calculations are also shown.

Semiconductor	a (au)	E_g^{exp} (eV)	d/i	ϵ	E_g^{theor} (eV)
Si	10.26	1.12	i	11.7	0.53
Ge	10.70	0.75	i	16.0	0.49
AlP	10.30	2.51	i	9.8	1.63
AlAs	10.61	2.21	i	10.1	1.47
AlSb	11.61	1.71	i	11.2	1.16
GaP	10.30	2.35	i	10.9	1.56
GaAs	10.68	1.52	d	12.5	1.38
GaSb	11.57	0.81	d	15.7	0.74
InP	11.09	1.42	d	12.6	1.67
InAs	11.45	0.41	d	15.2	0.59
InSb	12.26	0.24	d	16.8	0.42

The band gaps resulting from our calculations are also shown in table 1. The theoretical band gaps for the direct-gap semiconductors are rather large compared with other self-consistent LDA calculations. This is evidently due to the 'one-particle' approximations, i.e. the linearisation to second order in $(E - E_\nu)$ and the ASA. The treatment of the outermost d shell as core electrons may also affect the results in the case Ga and In compounds. For example, our LMTO ASA calculations to second order in $(E - E_\nu)$ give in the case of GaAs a gap of 1.38 eV. If the energy bands are corrected to third order, we obtain a narrower gap of 0.74 eV, which is in a better agreement with previous LMTO and pseudopotential calculations [21]. Previous LMTO calculations have shown that going beyond the ASA decreases the band gap and the most accurate, fully relativistic calculations give a band gap of only 0.25 eV. The situation in our calculations with these approximations is analogous to the pseudopotential Green function calculations with an incomplete plane-wave basis. Pseudopotential calculations of this type by Baraff and Schlüter [22] have also given a rather large

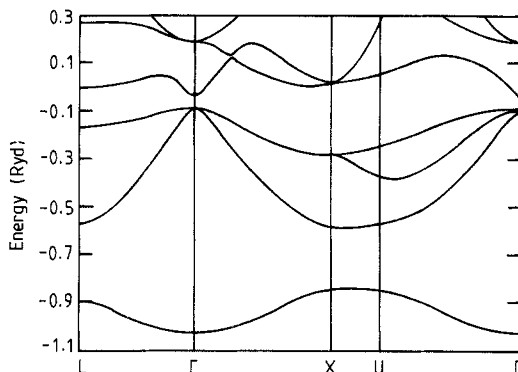

Figure 1. Scalar relativistic energy band structure for GaAs. The bands are calculated to second order in $E - E_\nu$ within the ASA.

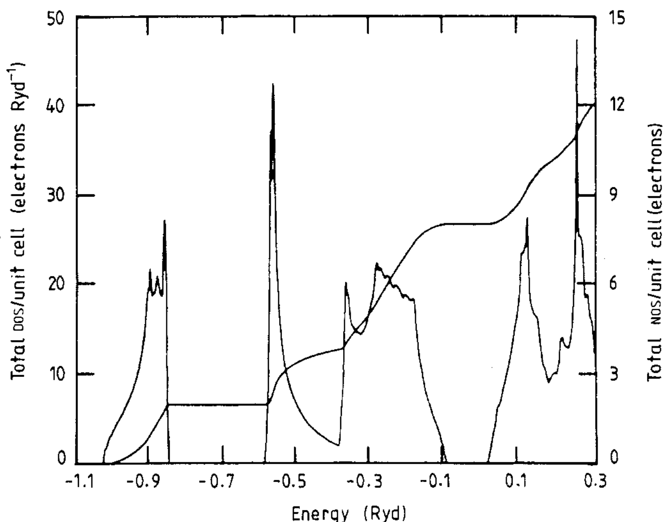

Figure 2. Density of states (DOS) and the integrated density of states (NOS) for GaAs. The energy scale is the same as in figure 1.

band gap and as a result they have omitted the scissors operator in consequent Green function calculations.

As an example of the electronic structures of III–V compound semiconductors the energy bands and the density of states for GaAs are shown in figures 1 and 2, respectively. The lowest band shown arises from the As 4s states. Above that there is the heteropolar energy gap and the valence band. In the density of states the lowest peak in the valence band at an energy of about −0.55 Ryd corresponds to mainly s-like states at the Ga site. The truncated peak in the upper part of the valence band is mainly due to the p-like states at the As site. The band gap is direct and the main character of the lowest states in the conduction band is s type at the Ga site.

3.2. Vacancies

The calculated change in the density of states due to the Ga vacancy in GaAs (V_{Ga}) is

shown in figure 3. The results correspond to a neutral vacancy and the majority spin. Actually, in this case the dependence on the spin is rather weak. Only the contributions belonging to the A_1 (s-like states at the vacancy) and T_2 (p-like states at the vacancy) representations of the T_d point group are shown. The other three representations contribute much less to the change in the DOS. For practical convenience the changes in the DOS have been drawn for energies with a small constant imaginary part. Therefore the features in figure 3 are smoothed and e.g. the bound states appear as peaks with finite widths.

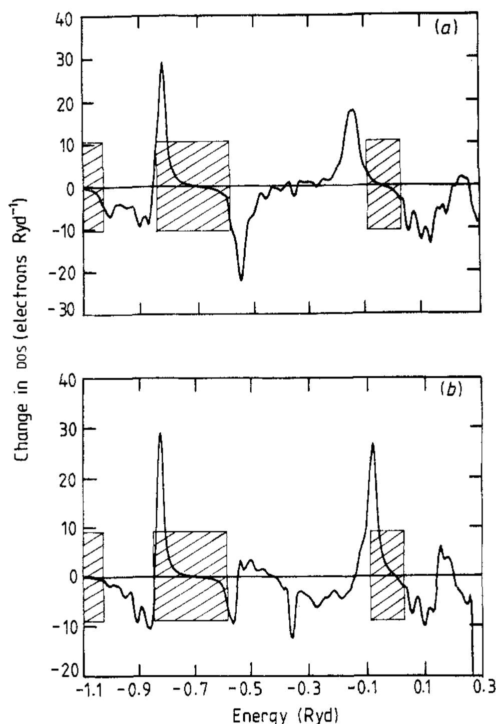

Figure 3. Changes in the density of states of (*a*) A_1 and (*b*) T_2 symmetries induced by a Ga vacancy in GaAs. The positions of the band gaps are given by shaded boxes. The energy scale is the same as in figure 1.

The Ga vacancy pushes the states to higher energies. In the A_1 representation s-like states are removed from the As 4s band and from the bottom of the valence band and states are added as a bound state in the heteropolar gap and as a resonance near the top of the valence band. The A_1 changes in the DOS integrate to zero over the valence band energies, which means that there is no net loss of A_1 electrons from the valence band due to the formation of a Ga vacancy. In the T_2 changes to the DOS the important feature is the removal of p-like states from the region below the top of the valence band and the appearence of a bound state (the peak inside the shaded box in figure 3), i.e. a deep level, in the band gap. The T_2 change in the DOS integrated up to the top of the valence band indicates the removal of six electrons from the valence band. Because the creation of a Ga vacancy means that three valence electrons are taken out of the system, a neutral Ga vacancy is obtained by the occupation of the bound T_2 state in the band gap by three electrons. By varying the occupancy of the

bound state different charge states of the vacancies are obtained. The change in the density of states due to the As vacancy is very similar to that given for the Ga vacancy in figure 3. The main difference is that the states are pushed more strongly upwards because of the larger size of the anion vacancy V_{As} compared with the cation vacancy V_{Ga}. As a consequence the bound T_2 state for the former is at the upper part of the band gap whereas the latter induces a bound state near the valence band edge. In order to obtain a neutral As vacancy one electron has to occupy the bound states. The electron structures of the vacancies in other III–V semiconductors are rather similar to those for vacancies in GaAs. Typically anion vacancies induce donor-type deep levels near the conduction band edge, whereas cation vacancies induce acceptor-type levels near the valence band edge.

The results for the positions of the ionisation levels for vacancies are collected in table 2. In Si and Ge vacancies there are several levels spread throughout the energy gap, and the vacancies can be negative, neutral or positive. The cation vacancies of the III–V compound semiconductors have ionisation levels in the lower half of the band gap. The cation vacancies exist only in negative or neutral states, except in AlP and AlAs, where the upward shift of the electron states due to the Al vacancy is so strong that there are also singly positive charge states. The anion vacancies are positive when the Fermi level is far from the conduction band. In the small-band-gap semiconductors InAs and InSb and in AlP cation vacancies do not reach the neutral state when the Fermi level is shifted towards the conduction band edge. Negative charge states exists for anion vacancies in AlSb, GaP, GaAs and GaSb. In the large-band-gap compounds AlP, AlAs, AlSb and GaP the anion vacancy pushes s-type states from the valence band to the band gap, and ionisation levels appear due to the change in the occupation of the A_1-symmetry deep level.

Table 2. Calculated positions of the ionisation levels in semiconductor vacancies. The energies are given relative to the top of the valence band. The symmetry of the one-particle energy level, the occupation of which is changing, is T_2, except in the few cases shown where it is A_1.

Semiconductor	Vacancy	Ionisation level	Energy (eV)	Symmetry
Si	V_{Si}	(+/2+)	0.45	
		(0/+)	0.55	
		(−/0)	0.66	
		(2−/−)	0.92	
		(3−/2−)	1.00	
Ge	V_{Ge}	(+/2+)	0.16	
		(0/+)	0.21	
		(−/0)	0.27	
		(2−/−)	0.42	
		(3−/2−)	0.49	
AlP	V_{Al}	(0/+)	0.24	
		(−/0)	0.66	
		(2−/−)	0.90	
		(3−/2−)	1.11	
	V_P	(2+/3+)	0.15	A_1
		(+/2+)	0.53	A_1

Table 2. (Continued)

Semiconductor	Vacancy	Ionisation level	Energy (eV)	Symmetry
AlAs	V_{Al}	(0/+)	0.20	
		(−/0)	0.53	
		(2−/−)	0.73	
		(3−/2−)	0.92	
	V_{As}	(2+/3+)	0.13	A_1
		(+/2+)	0.46	A_1
		(0/+)	2.11	
AlSb	V_{Al}	(−/0)	0.30	
		(2−/−)	0.42	
		(3−/2−)	0.55	
	V_{Sb}	(+/2+)	0.27	A_1
		(0/+)	1.36	
		(−/0)	1.46	
		(2−/−)	1.57	
GaP	V_{Ga}	(−/0)	0.32	
		(2−/−)	0.49	
		(3−/2−)	0.68	
	V_P	(+/2+)	0.24	A_1
		(0/+)	1.79	
		(−/0)	1.94	
		(2−/−)	2.08	
GaAs	V_{Ga}	(−/0)	0.11	
		(2−/−)	0.22	
		(3−/2−)	0.33	
	V_{As}	(0/+)	1.20	
		(−/0)	1.30	
		(2−/−)	1.39	
GaSb	V_{Ga}	(3−/2−)	0.17	
	V_{Sb}	(0/+)	0.70	
		(−/0)	0.77	
InP	V_{In}	(−/0)	0.14	
		(2−/−)	0.20	
		(3−/2−)	0.38	
	V_P	(0/+)	1.37	
InAs	V_{In}	(−/0)	0.10	
		(2−/−)	0.13	
		(3−/2−)	0.23	
	V_{As}	Always positive		
InSb	V_{In}	(3−/2−)	0.15	
	V_{Sb}	Always positive		

The distances between the adjacent ionisation levels in vacancies depend rather linearly on the width of the band gap. For the small-band-gap semiconductors studied the distance is about 0.05 eV whereas for the large-band-gap compounds it is over 0.2 eV. Our calculations are spin dependent and, according to Hund's rules, the spatially

triply degenerate T_2 states have been filled first by three spin-up electrons and thereafter the filling of spin-down states has been started. This spin dependence is reflected as a (1.5–2.5 times) larger gap between the ionisation levels when the first spin-down electron is introduced than in other changes to the charge state. Therefore there is a larger gap between the levels (−/0) and (2−/−) in Si and Ge. In III–V compounds this happens between (0/+) and (−/0) for cation vacancies, and is seen in the cases of AlP and AlAs. In cation vacancies this large gap should exist between (2−/−) and (3−/2−), but is not seen in our results because the latter level is pushed into the conduction band.

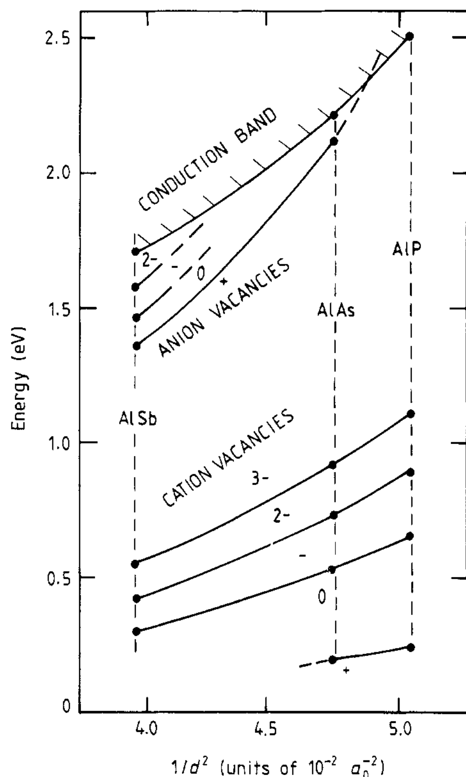

Figure 4. Bottom of the conduction band and the ionisation levels for anion and cation vacancies in AlP, AlAs, and AlSb relative to the top of valence band. The abscissa is the square of the inverse of the bond length d. The regions of different charge states are also shown.

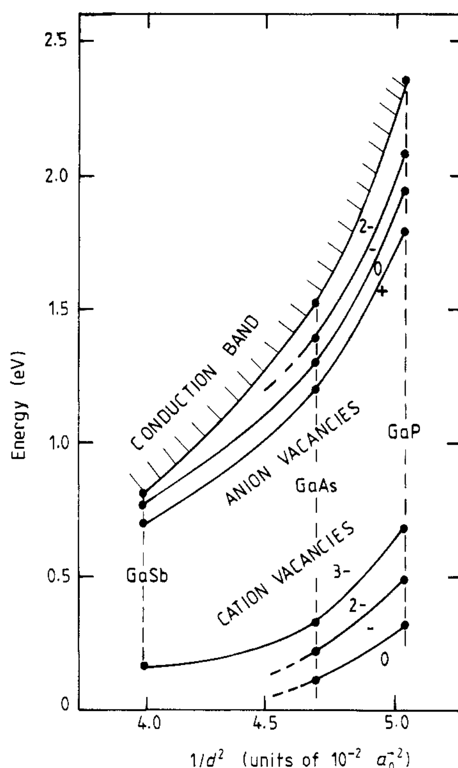

Figure 5. Same as figure 4 but for GaP, GaAs, and GaSb.

In order to study more carefully the trends in ionisation levels we have plotted in figures 4–6 the ionisation levels and the bottom of the conduction band relative to the top of the valence band as a function of the inverse square of the bond length d. According to the model by Harrison [23], the band gap widths should behave as d^{-2}. The trends are followed when the cation is kept the same and the anion is varied. The trends when the cation is changing cannot be plotted this way, because the 'size' of the anion determines the lattice constant when the cation is Al or Ga. Figures 4–6 show that the ionisation levels generally follow the same increasing trend as the bottom of

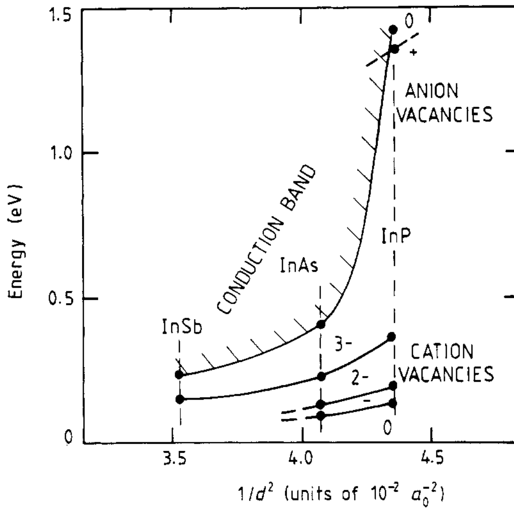

Figure 6. Same as figure 4 but for InP, InAs, and InSb.

the conduction band. In Al compounds the anion vacancy levels seem to rise faster than the bottom of the conduction band. One result from this tendency is that the P vacancy in AlP has only positive charge states. In Ga and In compounds the rise of the anion vacancy levels is similar to or even slower than the rise of the bottom of the conduction band. The most prominent consequence from this behaviour is that the anion vacancies in the narrow-gap semiconductors InSb and InAs are always positive. The different behaviour of the anion vacancy levels in Al compounds may reflect the fact that all these compounds have an indirect band gap whereas the other III–V compounds (except GaP) have a direct band gap, and thus the lowest energy states of the conduction band have different character in the two cases. This conclusion is supported by the trend shown by the uppermost ionisation levels in Si and Ge vacancies (see figure 7), because these semiconductors have an indirect band gap.

The cation vacancies have in all cases negative charge states. The vacancies in Al compounds push the ionisation levels upwards more strongly than vacancies in the other compounds. In other words, vacancies in Al compounds are seen to be stronger perturbations than vacancies in the Ga and In compounds. As a result Al vacancies in AlAs and AlP are found to exist also in a singly positive state.

3.3. Anti-site defects

The change in DOS due to the As_{Ga} anti-site in GaAs is shown in figure 8. In the As_{Ga} anti-site one Ga site is occupied by an As atom. As_{Ga} pulls states downwards. Therefore with the A_1 (s-type states at As) change in the DOS in figure 8 three bound states appear below the bottoms of different bands. The T_2 (p-type at As) change in the DOS also shows a lowering of the different states, but results in resonances above the band bottoms, where there are s-type states in the unperturbed system. The changes in the DOS integrate to zero over the valence band energies. Therefore, in order to obtain a neutral system, the A_1-type bound state in the band gap near the conduction band has to be occupied by two electrons. The other possible charge states are + and 2+. The Ga_{As} anti-site pushes states upwards in a similar way to vacancies. A T_2 state is

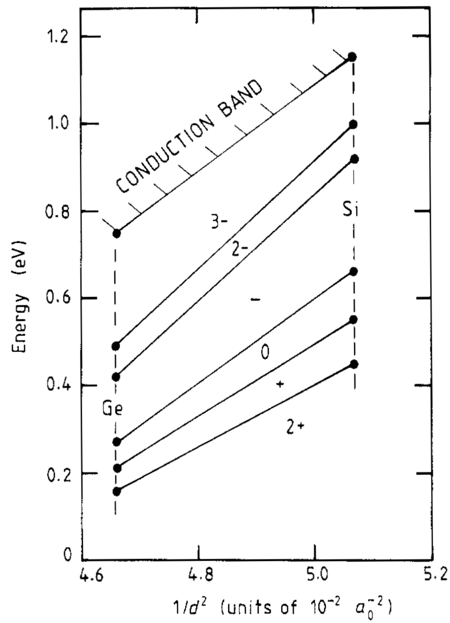

Figure 7. Same as figure 4 but for Si and Ge.

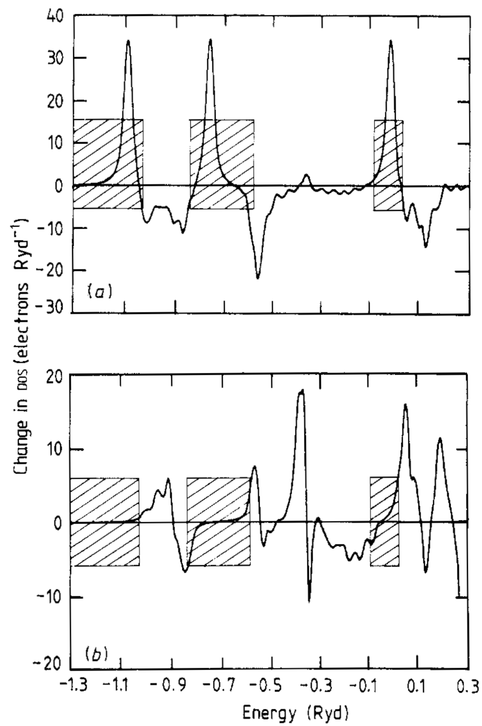

Figure 8. Changes in the density of states of (*a*) A_1 and (*b*) T_2 symmetries induced by a As_{Ga} anti-site in GaAs. The positions of the band gaps are given by shaded boxes. The energy scale is the same as in figure 1.

lifted to the band gap, and in a neutral defect it is occupied by four electrons. The electronic structures of anti-sites in other compound semiconductors are similar. Anion anti-sites (e.g. As_{Ga}) induce donor-type states whereas cation anti-sites (e.g. Ga_{As}) lead to acceptor-type states.

Table 3. Calculated positions of the ionisation levels for anti-site defects in semiconductors. The energies are given relative to the top of the valence band. The symmetry of the one-particle energy level, the occupation of which is changing, is T_2 or A_1 as shown.

Semiconductor	Anti-site	Ionisation level	Energy (eV)	Symmetry
AlP	Al_P	(+/2+)	0.17	T_2
		(0/+)	0.60	T_2
		(−/0)	0.84	T_2
		(2−/−)	1.12	T_2
	P_{Al}	(+/2+)	1.86	A_1
		(0/+)	2.15	A_1
AlAs	Al_{As}	(0/+)	0.41	T_2
		(−/0)	0.63	T_2
		(2−/−)	0.88	T_2
	As_{Al}	(+/2+)	1.64	A_1
		(0/+)	1.87	A_1
AlSb	Al_{Sb}	(0/+)	0.14	T_2
		(−/0)	0.25	T_2
		(2−/−)	0.40	T_2
	Sb_{Al}	(+/2+)	1.50	A_1
		(0/+)	1.62	A_1
GaP	Ga_P	(0/+)	0.30	T_2
		(−/0)	0.46	T_2
		(2−/−)	0.68	T_2
	P_{Ga}	(+/2+)	1.59	A_1
		(0/+)	1.83	A_1
GaAs	Ga_{As}	(−/0)	0.11	T_2
		(2−/−)	0.28	T_2
	As_{Ga}	(+/2+)	0.88	A_1
		(0/+)	1.07	A_1
GaSb	Ga_{Sb}	Charge state −2		
	Sb_{Ga}	Charge state +2		
InP	In_P	(0/+)	0.24	T_2
		(−/0)	0.36	T_2
		(2−/−)	0.51	T_2
	P_{In}	(0/+)	0.44	A_1
InAs	In_{As}	(0/+)	0.12	T_2
		(−/0)	0.21	T_2
		(2−/−)	0.32	T_2
	As_{In}	Charge state 0		
InSb	In_{Sb}	(2−/−)	0.11	T_2
	Sb_{In}	Charge state +2		

The results for the ionisation levels induced by the anti-site defects are collected in table 3. Cation anti-sites push a T_2-symmetry state into the band gap. The perturbation is strongest in the large band gap semiconductors as in the case of vacancies. The weakest perturbation is seen to be due to the Ga_{Sb}, for which the T_2 states form a resonance in the valence band and the defect has only the doubly negative charge state. Anion anti-sites pull an A_1-symmetry state from the conduction band into the band gap. The efficiency of pulling the state downwards decreases as the size of the anion increases in the sequence P–As–Sb. Sb anti-sites in GaSb and InSb are not able to pull states into the band gap and therefore they are always in the doubly negative state. One interesting prediction of the present calculations is that in GaSb there are no deep levels due to anti-site defects.

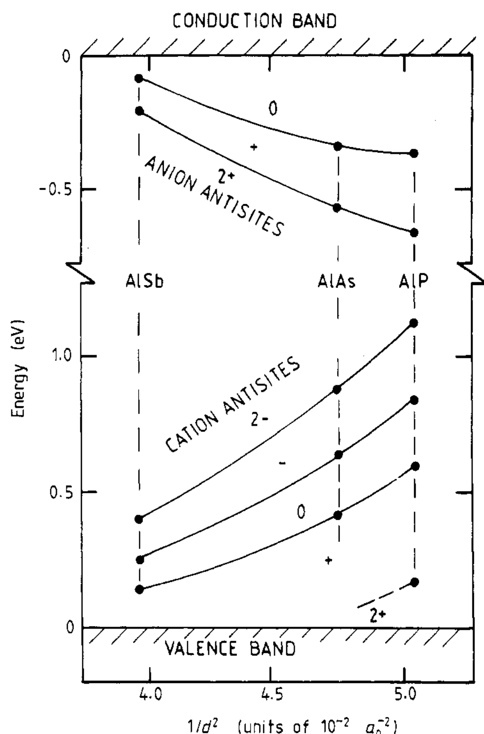

Figure 9. Ionisation levels for cation and anion anti-sites in AlP, AlAs and AlSb. The levels for the cation anti-sites are shown relative to the top of the valence band and for anion anti-sites relative to the bottom of the conduction band. The abscissa is the square of the inverse of the bond length d. The regions of different charge states are also shown.

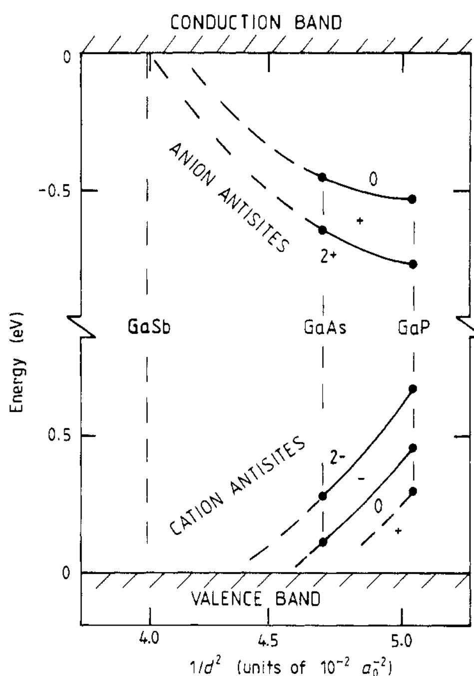

Figure 10. Same as figure 9 but for GaP, GaAs, and GaSb.

In order to see the trends more clearly the ionisation levels are plotted in figures 9–11 as a function of the inverse square of the bond length. The levels due to the cation anti-sites are plotted relative to the top of the valence band, whereas the reference for levels induced by the anion anti-sites is the bottom of the conduction band. The ionisation levels show smooth trends confirming that the results corresponding to different hosts are consistent with each other. The main trend is that the ionisation

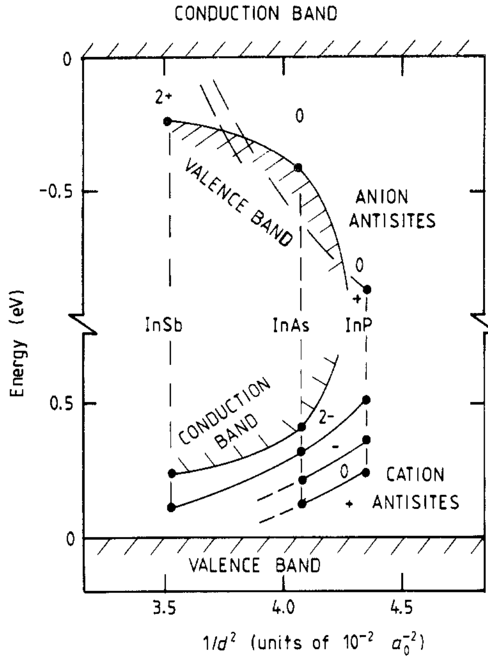

Figure 11. Same as figure 9 but for InP, InAs, and InSb.

levels are pushed further away from the band edges when the band gap increases. Figure 11 explains nicely why it is possible that As_{In} is always neutral, whereas Sb_{In} has only the doubly positive charge state.

3.4. Comparison with previous theoretical and experimental results

In the case of point defects in semiconductors the first self-consistent electron structure calculations based on the Green function method were performed about one decade ago for the ideal neutral vacancy in silicon [24, 25]. The calculations used pseudopotentials and the important result obtained was that there exists a deep doubly occupied bound state slightly above the middle of the gap. This feature is reproduced by our calculations, too. However, according to the present understanding [3, 26] the real situation is more complicated, due to the influence of ionic relaxation on the electron states. When there are no electrons on the deep levels, i.e. in the case of V_{Si}^{2+}, only symmetry-conserving breathing relaxation occurs and the symmetry group is T_d. In the case of V_{Si}^{+} there is one electron on a deep level and a tetragonal relaxation lowers the symmetry to D_{2d}. The driving force behind this relaxation is the Jahn–Teller effect in which the symmetry lowering removes the spatial degeneracy of the deep levels and the total energy of the defect decreases. The second electron added leads to a neutral state V_{Si}^{0}. It has the opposite spin relative to the other electron, and therefore the symmetry remains D_{2d}, although the magnitude of the displacements may change. In the negative state V_{Si}^{-} the symmetry is lowered to C_{2v} due to a mixture of tetragonal and trigonal relaxations. When the Fermi level rises in the band gap the occupancy of the deep levels changes and the above processes take place. However, according to theoretical [27] and experimental [26] considerations V_{Si} forms a so-called negative effective-U system. This means that due to the relaxation the total energy for the system V_{Si}^{0} with two deep

electrons is lower than that for V_{Si}^{+}, which has only one localised electron. As a result the ionisation level (0/+) lies below the level (+/2+). The effects of relaxation, which is not taken into account our calculations, are to lower the positions of the deep levels, remove the degeneracies and even change the relative ordering of the levels. Therefore the detailed comparison of our theoretical predictions with experimental results may not be very meaningful. The worth of our results is more on the trends they show. For example, the theoretical and experimental values of the deep levels are shown in table 4.

Table 4. Comparison of theoretical and experimental ionisation levels for the Si vacancy. The energies are given relative to the top of the valence band.

Ionisation level	Energy (eV)	
	Present theory	Experiment
(+/2+)	0.45	0.13[a]
(0/+)	0.55	0.05[a]
(−/0)	0.66	0.42[b]
(2−/−)	0.92	0.88[b]
(3−/2−)	1.00	

[a] [28].
[b] [29].

It is seen that experimental values for the (+/2+) and (0/+) levels are close to the top of the valence band whereas our values are in the mid-gap region. However, it is interesting to note that when the occupancy of the deep levels increases, the discrepancy between the theoretical and experimental values decreases. This probably reflects the fact that the magnitude of the outward relaxation of the vacancy decreases when the number of bound electrons increases [6, 27, 30]. Thus our predictions, which assume no relaxation, should be the better the more negative the vacancy is.

From the systems considered in this work, point defects in GaAs have attracted the most theoretical and experimental studies. We have compared our present calculations for the ionisation levels with different theoretical and experimental results in table 5. Results for vacancies and for the anti-site defects As_{Ga} and Ga_{As} are included.

The first self-consistent Green function calculations for vacancies and As_{Ga} anti-sites in GaAs were performed by Bachelet *et al* [31, 32] employing the pseudopotential method. They found that neutral Ga and As vacancies both induce a T_2-type bound state with *one-particle energy eigenvalue* of 0.06 eV (V_{Ga}^{o}) and 1.08 eV (V_{As}^{o}) above the top of the valence band. Our corresponding values, 0.08 eV for V_{Ga}^{o} and 1.20 eV for V_{As}^{o} agree well with these result. Bachelet *et al* did not calculate the ionisation levels for the vacancies. For the As_{Ga} anti-site they estimated the ionisation levels (+/2+) and (0/+) to lie at 0.83 eV and 1.10 eV, respectively (table 5) [32]. These values are in a very good agreement with our results of 0.88 eV and 1.07 eV. In a subsequent calculation Baraff and Schlüter [19] used a more accurate method to calculate the charge states and Coulomb tails and as a result all the energy levels were pushed upwards by about 0.4 eV. For instance, according to these calculations V_{As} should always be positive. Thus, their new values shown in table 5 do not agree with our results.

We have also included in table 5 experimental data for ionisation levels at point defects in GaAs, which can be compared with the theoretical results. On the basis of the deep-level optical spectroscopy measurements it has been suggested that V_{As} has (2−/−) and (−/0) levels at 0.04 eV and 0.18 eV below the bottom of the conduction

Table 5. Comparison of theoretical and experimental ionisation levels for point defects in GaAs. The energies (in eV) are given relative to the bottom of the conduction band in the case of V_{As} and relative to the top of the valence band in the other cases.

Defect	Ionisation level	Theoretical results: Present work	Theoretical results: Previous works		Experimental results		
V_{Ga}	(−/0)	0.11		~0.2[a]			
	(2−/−)	0.22		~0.5[a]			
	(3−/2−)	0.33		~0.7[a]			
V_{As}	(−/0)	−0.22		Always	−0.18[b]	−0.14[c]	−0.10[d]
	(2−/−)	−0.13		positive[a]	−0.04[b]	−0.045[c]	−0.035[d]
As_{Ga}	(+/2+)	0.88	0.83[e]	1.25[a]	0.52[f]		
	(0/+)	1.07	1.10[e]	1.50[a]	0.75[f]		
Ga_{As}	(−/0)	0.11		0.30[a]	0.077[g]	0.40[h]	
	(2−/−)	0.28		0.62[a]	0.23[g]	0.70[h]	

[a] [19]. [e] [32].
[b] [33]. [f] [35].
[c] [34]. [g] [36].
[d] [7]. [h] [37].

band, respectively [33]. The interpretation of DLTS data gives similar results: 0.045 eV and 0.14 eV [34]. According to recent positron lifetime experiments the levels (2−/−) and (−/0) are connected with energies of 0.035 eV and 0.10 eV below the bottom of the conduction band, respectively [7]. The positron lifetime measurements should be especially relevant, because they are sensitive only to negative- (and maybe neutral-) vacancy defects, and e.g. interstitial or anti-site defects can be excluded from the interpretation. Our theoretical results, 0.22 eV for (−/0) and 0.13 eV for (2−/−) measured from the bottom of the conduction band are very close to the experimental values. This is somewhat surprising because one would expect a larger deviation due to ionic relaxation as in the case of the lowest ionisation levels in Si. Moreover, now the theoretical results seem to lie about 0.1 eV *below* the experimental ones.

A possible reason for this good agreement between the theoretical and experimental results is that the relaxation of the As vacancy in GaAs has a different character compared with the vacancy in Si. This conclusion is also supported by the fact that the negative effective-U behaviour is not seen for the vacancies in GaAs. However, in this experiment–theory comparison as well as in those below one should bear in mind that the scissors operator used can have a remarkable effect on the detailed conclusions. There exist no experimental data for ionisation levels in the Ga vacancy. This is probably due to its suggested instability prior to the recombination with Ga interstitials or to the change to a V_{As}–As_{Ga} configuration.

The comparison of the experimental and theoretical values for the As_{Ga} anti-site indicates somewhat larger relaxation effects. Namely, according to the measurements [35] the ionisation levels (+/2+) and (0/+) lie at energies 0.52 eV and 0.75 eV above the valence band, whereas our results are 0.88 eV and 1.07 eV, respectively. For the Ga_{As} anti-site there are controversial experimental results. Yu *et al* [36] give energies of 0.077 eV and 0.23 eV from the top of the valence band for the ionisation levels (−/0) and (2−/−), respectively. These results are consistent with our values of 0.11 eV and 0.28 eV, and the comparison indicates nicely a small effect due to the ionic relaxation.

The experimental values by Wang *et al* [37] are at much higher energies, i.e. at 0.40 eV and 0.70 eV. Our results for both types of anti-sites and the experimental results, excluding the values by Wang *et al*, are consistent with each other with respect to the effects of the relaxations one expects to happen. Namely, the relaxation connected with the Ga_{As} anti-site should be small, because the 'larger' anion, As, determines the lattice constant of the perfect crystal, and thus no large distortion is expected when the 'large' As atom is substituted by the 'small' Ga atom. On the other, when the 'small' Ga atom is substituted by the 'large' As atom in order to create the As_{Ga} anti-site it is natural that the distortion is large. Finally, it is also very satisfying to note that the calculations can reproduce the experimental separation between the ionisation levels in As_{Ga} and also in $GaAs_{AsGa}$ if one compares with the results by Yu *et al*.

4. Conclusions

We have systematically studied the ionisation levels of ideal vacancies and anti-site defects in III–V compound semiconductors by self-consistent electronic structure calculations. The cation vacancies induce acceptor-type levels in the band gap near the top of the valence band whereas anion vacancies induce donor-type levels near the top of the conduction band. Typically, cation vacancies have negative charge states and anion vacancies are usually positive, but when the Fermi level is near the conduction band, anion vacancies may also have negative charge states. The positions of the ionisation levels relative to the top of the valence band rise when the energy gap increases as a function of the inverse of the bond length. The rise of the donor-type levels is faster in indirect-band-gap semiconductors than the rise of the bottom of the conduction band. The opposite trend is true for the direct-band-gap semiconductors. Due to these differences in the behaviour of the donor levels, some of these levels may emerge into the conduction band in large-indirect-band-gap and in small-direct-band-gap semiconductors. As a result, anion vacancies in these cases end up having only positive charge states. The perturbations due to vacancies are seen to become stronger when the band gap of the semiconductors is larger. In large-band-gap semiconductors acceptor-type ionisation levels at cation vacancies are pushed deep into the gap and a positive charge state may appear.

The cation anti-sites push up T_2-symmetry states from the valence band and the anion anti-sites pull down A_1-symmetry states from the conduction band. As a result, the former usually induce acceptor-type levels in the band gap near the top of the valence band and the latter induce donor-type defects near the bottom of the conduction band. However, the actual details depend strongly on the width of the band gap and on the relative size of the anti-site atom.

The comparison of our theoretical results with available experimental data shows, within the uncertainty caused by the scissors operator, the effects due to lattice relaxation. According to the experiments the lowest ionisation levels for a vacancy in Si are much lower in the band gap than according to our calculations for an ideal vacancy. However, the agreement is much better for the higher ionisation levels, which should be affected by a smaller relaxation. Also in the case of anti-sites in GaAs the experimental and theoretical results are very close to each other for Ga_{As}, which is expected to be only slightly distorted. However, in the case of As_{Ga}, which should show larger relaxation effects, the experimental ionisation levels lie considerably lower than the theoretical ones. Finally, according to experiments and our calculations for the As

vacancy in GaAs there are ionisation levels near the bottom of the conduction band. The experimental and theoretical values are rather near each other, which means that the relaxation around an As vacancy is not large, at least in comparison with positive and neutral vacancies in Si.

Acknowledgments

We are grateful to P Hautojärvi and R M Nieminen for many helpful discussions.

References

[1] *Proc. 14th Int. Conf. on Defects in Semiconductors, Paris 1986* ed. H J von Bardeleben (1986 *Mater. Sci. Forum* **10–12**)

[2] *Proc. 15th Int. Conf. on Defects in Semiconductors, Budapest 1988* to be published

[3] Lannoo M and Bourgoin J 1981 *Point Defects in Semiconductors I* Springer Series in Solid State Sciences **27** (Berlin: Springer)
Bourgoin J and Lannoo M 1983 *Point Defects in Semiconductors II* Springer Series in Solid State Sciences **35** (Berlin: Springer)

[4] Pantelides S T (ed.) 1986 *Deep Centers in Semiconductors* (New York: Gordon and Breach)

[5] Scheffler M, Vigneron J P and Bachelet G P 1985 *Phys. Rev.* B **31** 6541

[6] For reviews, see e.g. Dlubek G and Krause R 1987 *Phys. Status Solidi* a **102** 443
Dannefaer S 1987 *Phys. Status Solidi* a **102** 481

[7] Corbel C, Stucky M, Hautojärvi P, Saarinen K and Moser P 1989 *Phys. Rev.* B in press

[8] Andersen O K, Jepsen O and Glötzel D 1985 *Highlights of Condensed-Matter Theory* ed. F Bassani, F Fumi and M P Tosi (Amsterdam: North-Holland) p 59

[9] Skriver H L 1984 *The* LMTO *Method* (New York: Springer)

[10] Gunnarsson O, Jepsen O and Andersen O K 1983 *Phys. Rev.* B **27** 7144

[11] Beeler F, Scheffler M, Jepsen O and Gunnarsson O 1985 *Phys. Rev. Lett.* **54** 2525

[12] Beeler F, Andersen O K and Scheffler M 1985 *Phys. Rev. Lett.* **55** 1498

[13] Puska M J, Jepsen O, Gunnarsson O and Nieminen R M 1986 *Phys. Rev.* B **34** 2695

[14] Baraff G A and Schlüter M 1984 *Phys. Rev.* B **30** 3460

[15] Ceperley D M and Alder B J 1980 *Phys. Rev. Lett.* **45** 566; we use their local exchange-correlation functional as parametrised by Perdew J and Zunger A 1981 *Phys. Rev.* B **23** 5048

[16] Perdew J P and Levy M *Phys. Rev. Lett.* **51** 1884
Sham L J and Schlüter M 1983 *Phys. Rev. Lett.* **51** 1888; 1985 *Phys. Rev.* B **32** 3883

[17] Godby R W, Schlüter M and Sham L J 1988 *Phys. Rev.* B **37** 10159

[18] Rodriquez C O, Brand S and Jaros M 1980 *J. Phys. C: Solid State Phys.* **13** L333

[19] Baraff G A and Schlüter M 1985 *Phys. Rev. Lett.* **55** 2340

[20] Madelung O (ed.) 1982 *Landolt-Börnstein, Numerical Data and Functional Relationships in Science and Technology* vol 17a (Berlin: Springer)
Wyckoff R W G 1982 *Crystal Structures* vol 1 (Malabar: Krieger)

[21] Bachelet G B and Christensen N E 1985 *Phys. Rev.* B **31** 879

[22] Baraff G A and Schlüter M 1987 *Phys. Rev.* B **35** 6154

[23] Harrison W A 1987 *Comment. Condens. Matter Phys.* **13** 207

[24] Baraff G A and Schlüter M 1978 *Phys. Rev. Lett.* **41** 892; 1979 *Phys. Rev.* B **19** 4965

[25] Bernholc J, Lipari N O and Pantelides S T 1978 *Phys. Rev. Lett.* **41** 895; 1980 *Phys. Rev.* B **21** 3545

[26] Watkins G 1986 *Deep Centers in Semiconductors* ed S T Pantelides (New York: Gordon and Breach) p 147

[27] Baraff G A, Kane E O and Schlüter M 1979 *Phys. Rev. Lett.* **43** 956; 1980 *Phys. Rev.* B **21** 3563; 5662

[28] Newton J L, Chatterjee A P, Harris R D and Watkins G D 1983 *Physica* B **116** 219

[29] Watkins G D 1975 *Lattice Defects in Semiconductors 1974* (Inst. Phys. Conf. Ser. 23)

[30] Samara G A 1987 *Phys. Rev.* B **37** 8523

[31] Bachelet G B, Schlüter M and Baraff G A 1981 *Phys. Rev.* B **24** 915

[32] Bachelet G B, Schlüter M and Baraff G A 1983 *Phys. Rev.* B **27** 2545

[33] Loualiche S, Nouailhat N, Guillot G and Lannoo M 1984 *Phys. Rev.* B **30** 5822
[34] Pons D and Bourgoin J C 1985 *J. Phys. C: Solid State Phys.* **18** 3839
[35] Weber E R *et al* 1982 *J. Appl. Phys.* **53** 6140
[36] Yu P W *et al* 1982 *Appl. Phys. Lett.* **41** 532
[37] Wang Z G, Ledebo L A and Grimmeiss H G 1984 *J. Phys. C: Solid State Phys.* **17** 259